remote sensing

MDPI

Article

Variability of Particle Size Distributions in the Bohai Sea and the Yellow Sea

Zhongfeng Qiu [1,2], Deyong Sun [1,2,*], Chuanmin Hu [3], Shengqiang Wang [1,2], Lufei Zheng [1], Yu Huan [1] and Tian Peng [1]

1 School of Marine Sciences, Nanjing University of Information Science & Technology, Nanjing 210044, China; zhongfeng.qiu@nuist.edu.cn (Z.Q.); wsqiang815@163.com (S.W.); lufei.z@outlook.com (L.Z.); yuhuan2406@163.com (Y.H.); wspp156@126.com (T.P.)

2 Jiangsu Research Center for Ocean Survey Technology, Nanjing 210044, China

3 College of Marine Science, University of South Florida, 140 Seventh Avenue South, St. Petersburg, FL 33701, USA; huc@usf.edu

* Correspondence: sundeyong1984@163.com; Tel.: +86-25-586-95698

Academic Editors: Deepak R. Mishra, Xiaofeng Li and Prasad S. Thenkabail
Received: 28 July 2016; Accepted: 9 November 2016; Published: 15 November 2016

Abstract: Particle size distribution (PSD) is an important parameter that is relevant to many aspects of marine ecosystems, such as phytoplankton functional types, optical absorption and scattering from particulates, sediment fluxes, and carbon export. However, only a handful of studies have documented the PSD variability in different regions. Here, we investigate the PSD properties and variability in two shallow and semi-enclosed seas (the Bohai Sea (BS) and Yellow Sea (YS)), using in situ laser diffraction measurements (LISST-100X Type C) and other measurements at 79 stations in November 2013. The results show large variability in particle concentrations (in both volume and number concentrations), with volume concentrations varying by 57-fold. The median particle diameter (D_v^{50}) from each of the water samples also covers a large range (22.4–307.0 μm) and has an irregular statistical distribution, indicating complexity in the PSD. The PSD slopes (2.7–4.5), estimated from a power-law model, cover nearly the entire range reported previously for natural waters. Small mineral particles (with large PSD slopes) are characteristic of near-shore waters prone to sediment resuspension by winds and tides, while large biological particles (with small PSD slopes) dominate the total suspended particulates for waters away from the coast. For the BS and YS, this study provides the first report on the properties and spatial variability of the PSD, which may influence the optical properties of the ocean surface and remote sensing algorithms that are based on estimations of particle concentrations and sizes.

Keywords: particle size; PSD slope; Junge distribution; LISST; Bohai Sea; Yellow Sea

1. Introduction

Suspended particles in marine environments play an important role by affecting the marine ecosystem, environment, and biogeochemistry, which may in turn be used to understand the natural and anthropogenic influences on the Earth's global systems [1,2]. One important parameter used to describe suspended particles is the particle size distribution (PSD), which is a measure of the particle concentrations (in either volume or number) at difference sizes. The PSD measure has been widely used to characterize marine particles [3].

PSD provides important information about the structure and functioning of aquatic ecosystems and is therefore of particular importance in many research fields of oceanography [4]. For instance, phytoplankton functional types usually vary with size, a finding that has been incorporated into global biogeochemical models and used to assess the ecological feedback to the ocean's carbon

cycle [5,6]. In ocean optics, PSD plays an important role in light propagation, light attenuation, and light reflection, which modulate the remote sensing signals of satellite sensors [7–10]. Both absorption and scattering of particles depend strongly on particle size and refractive index, although particle concentration is usually regarded as a primary factor [11]. In addition, PSD also plays an important role by affecting sediment fluxes, resuspension, aggregates, particle settling rates, and carbon export [12–14]. Therefore, it is of great interest and significance to document the properties and variability of the PSD in marine environments.

The constituents of water in marine environments cover an extremely broad size range that spans many orders of magnitude, from a molecular size on the order of 0.1 nm to large organisms that are several meters long [15–18]. Ocean optics are concerned with a size range from 0.01 to 1000 μm, encompassing viruses, bacteria, picoplankton, nanoplankton, microplankton, small meso-zooplankton, and sediments [16,17]. These constituents are generally divided into dissolved and particulate parts by using 0.2 μm as a threshold. The size of the distribution of the dissolved materials has rarely been reported. The size of the structure of the particulate materials (often called suspended particles, >0.2 μm in size) is of great interest to researchers. PSD measurements can resolve only a limited size range, and no study has yet reported information over the entire optically relevant size range [2]. Due to technique limitations, it is still difficult to conduct PSD measurements in the submicron range [19], while large particles with diameters above a few hundred microns are also hard to observe. In these cases, camera-based systems may be used [20,21].

Current methods for PSD measurements, such as the Coulter Counter (1–120 μm) and FlowCAM (5–100 μm), can provide information on particle sizes ranging from several microns to more than a hundred microns [2]. Another example is the LISST (Laser In-Situ Scattering and Transmissometry; Sequoia Scientific, Inc., hereafter referred to simply as LISST) instrument, which focuses on two size ranges, 1.25–250 μm (Type B) and 2.5–500 μm (Type C). Such instruments have been successfully applied in marine waters to explore particulate optical scattering [22], phytoplankton assemblages [23], complex water type discrimination [24], suspended floc size and settling rates [14].

PSD in marine environments can be influenced by many physical and biogeochemical processes; for instance, the dynamics of PSD in marine environments can be influenced by tidal current, waves and turbulence [25–28]. Numerous approximations have been proposed to describe PSD shapes in marine systems, such as power law models, Gaussian or lognormal distributions, variable-β models, two-parted Pareto distributions, Weibull distributions, characteristic vectors, and the gamma function [3,16,29–33]. Of these approximations, the power law model, also known as the "Junge distribution", is the most frequently used representation of PSD shapes [2,4,9–11,34]. Many processes in marine systems follow the power law, for instance, sea spray, bubble concentrations, sediments and organismal energetics [3,35,36]. Additionally, the theoretical justification for the applicability of the power law to aquatic suspended particles has been examined in previous studies [37,38]. The power law model has been considered a good first-order approximation for oceanic particles over several orders of magnitude [34].

The PSD slope, an important parameter describing the PSD, can be estimated by the power law approximation. The slope parameter provides information on the contribution of particles of different sizes to the total particles in a water sample. The greater the PSD slope, the higher proportion of small particles [2,20,34]. However, little is known about spatial and temporal variations in PSDs because of limited observations on either a macroscopic global or a microscopic regional scale. While global characterization depends on satellite-borne platforms and accurate retrieval algorithms [1], regional variations in PSD have been reported in several field-based investigations in locations, such as Monterey Bay (California, USA) [2], the Eastern Mediterranean Sea [39], and Hudson Bay (Canada) [4]. In general, there is a need to measure, report, and understand the variations in PSD in different marine environments. Additionally, the simple power-law model that describes the PSD slope needs to be validated across the full range of particle sizes [2,11].

In this study, we investigate the variability in PSD in two typically shallow and semi-enclosed seas, the Bohai Sea (BS) and the Yellow Sea (YS), with the following two objectives: (1) to model the PSD of the surface waters; and (2) to characterize the spatial variability and vertical distributions of the PSD. The potential findings by this study are very significant for understanding and documenting the particle size distributions in the BS and the YS, which have been regarded as important factors influencing water inherent optical properties [11,40–43], and further changing water color remote sensing signals [44].

2. Data and Methods

2.1. Study Area and Sampling

The cruise survey was conducted between 6 and 24 November 2013. The BS and the YS are typical shallow, semi-enclosed seas with Case II waters (i.e., optical properties are dominated by the water constituents, including non-algal particles, colored dissolved organic matter, and phytoplankton) as defined by Morel and Prieur (1977) [45]. The BS is the largest inner sea of China, covering a total area of approximately 77,000 km^2. Its average water depth is 18 m, with the maximum depth of approximately 70 m in the north of the Bohai Strait, the only passage to the YS [46]. The YS has an area of approximately 380,000 km^2 with average and maximum depths of approximately 44 and 140 m, respectively [47,48]. It can be roughly divided into two parts, the North Yellow Sea (NYS) and the South Yellow Sea (SYS).

The BS receives a large amount of suspended sediment loads from more than 17 rivers (e.g., the Yellow River). This leads to high concentrations of total suspended sediment matter (TSM). In the BS and YS, variations in the ocean hydrography, ocean circulation, sea surface temperature (SST), ocean stratification, and ocean fronts show significant seasonal characteristics. During the winter, the water is usually very turbid with a relatively high TSM, reaching approximately 100 $g \cdot m^{-3}$ for some regions of the BS and the YS, while during the summer, the TSM ranges from 10 to 20 $g \cdot m^{-3}$ [49]. Seasonal winds, ocean stratification, and sea surface thermodynamics due to seasonal climate change, as well as coastal bathymetry, seasonal phytoplankton blooms, and river discharges are the driving factors of the variations in the TSM [50].

Over the past several decades, the rapid proliferation of surrounding industries, agriculture, aquaculture and domestic sewage have made the BS a highly productive water region [46]. Similarly, the YS is also influenced by industrial pollution, agricultural runoff, and domestic sewage [51]. Abundant nutrients and sediments from rivers and non-point sources exported to the YS, together with the effects of winds and tides, lead to low water transparency in the region.

The data used in this study were collected from 79 stations during the winter 2013 shared voyage of state funds of China in the Bohai Sea (BS) and the Yellow Sea (YS) (Figure 1). At each station, a Sequoia LISST-100X was slowly lowered at a speed of approximately 0.15 m/s into the water column, to a depth that was slightly higher than the bottom 2–3 m to prevent damage to the instruments in the optical profiling package, and the sampling rate was 1 Hz (for more details, see references [52–59]). The LISST instrument was used to measure the size spectra of particles up to 500 μm in size. Observations made using the LISST instrument often suffer from light contamination and/or schlieren, which can significantly disrupt the measurement results [52]. In our actual measurement, LISST was fixed to a black iron rack horizontally to avoid man-made light. Due to the perturbations of the water environment, only downcast measurements were deemed valid and were used in the subsequent data analyses.

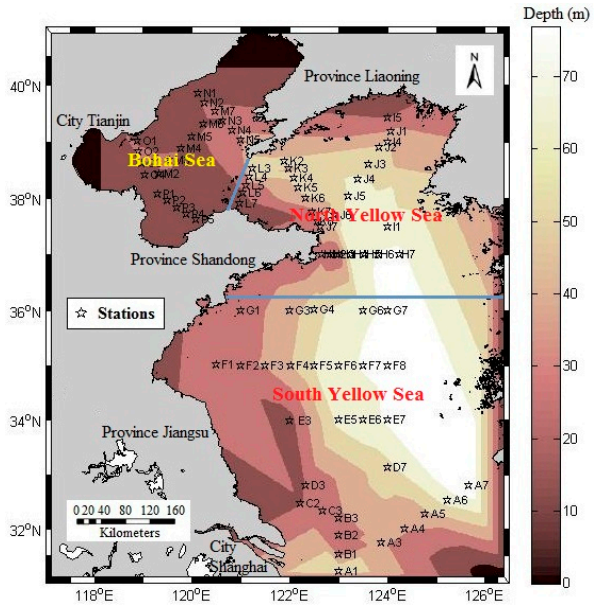

Figure 1. The study area and stations in the Bohai Sea and the Yellow Sea during the winter 2013 cruise. Bathymetric contours are color coded (n = 79, measured only once).

2.2. LISST Measurement

The PSD measurements were performed by using an LISST-100X Type-C particle size analyzer. The LISST is a commercially available instrument that measures the light scattering of a particle suspension at small forward angles and utilizes this information to estimate the PSD [54]. The theoretical foundation is that the optical diffraction by spherical particles whose diameters are significantly larger than the wavelength is assumed to be equivalent to the diffraction by an equal-sized aperture (Fraunhofer diffraction). Many studies have shown that LISST is capable of providing accurate estimates of PSD for various particle suspensions from inland lakes and marine waters [23,24,53–59].

The LISST instrument has 32 size ranges that are logarithmically distributed across a continuous size spectrum from 2.5 to 500 μm [51,60,61]. The upper size in each bin is 1.18 times that of the lower bin, and the width of the individual size classes varies from 0.45 to 76 μm. Scattered light in the near forward angles is measured on concentric detector rings, and inversion modeling based on Mie theory yields the particle volume concentration, V(D) (in μL/L), for the 32 size ranges [54]. For each size bin, there is an equivalent size, D (in μm), that is assumed to form a volume-equivalent sphere relative to the unknown particle shape. It is actually the geometric average of the upper and lower sizes of each size range. As noted in previous studies [11,62,63], LISST measurements at the smallest and largest size ranges may be not very steady due to the presence of particles outside of the measured size range. Thus, data of the smallest and largest size ranges were removed in the subsequent analysis. Prior to the LISST deployment, a background measurement was performed using MilliQ water for device calibration and subsequent data processing. The V(D) data were derived using the manufacturer-provided software LISST-SOP [61]. The particle number concentration, N(D) (in count/m^3), could be derived by dividing the volume concentration measured for each size bin by the volume of a sphere of the same diameter to obtain numbers of equivalent spherical diameter for each size bin. The inversion equation was as below

$$\mathrm{N(D)} = 6\mathrm{V(D)}/\pi\mathrm{D}^3 \quad (1)$$

The PSD, expressed as N'(D) (in count m^{-3} μm^{-1}), can be defined as the average number of particles within a given size class of width ΔD for a unit volume of suspension [2,4,16]

$$\mathrm{N'(D)} = \mathrm{N(D)}/\Delta\mathrm{D} \quad (2)$$

The PSD is thus different from the particle number concentration. When changing the given width of a particle size class, the PSD would vary accordingly, even for the same sample, whereas the particle number concentrations do not vary for the given particle sizes.

In addition to the near-forward scattering of a laser beam measured with a series of 32 annular detectors that spanned the approximate angular range of 0.08°–13.5° in the water over a path length of 5 cm (which is inverted to provide particle size information), an additional photodiode detector placed behind a centered hole was used to measure the transmitted light, from which the beam attenuation coefficient of particles (c_p, in m^{-1}) at 670 nm was calculated.

2.3. Methods to Characterize PSDs

In this study, the power law function was used to describe the PSD slope. Because one function form sometimes cannot capture the full complexity of the PSD [2,4,11,29,34], two power-law models, without and with correction of the parameters (see Equations (3) and (4)), were combined to describe the PSD in the study region:

$$N'(D) = N'(D_0)\left(\frac{D}{D_0}\right)^{-\xi} \quad (3)$$

$$N'(D) = \omega N'(D_0)\left(\frac{D}{D_0}\right)^{-\xi} \quad (4)$$

where D_0 is a reference diameter (in μm) and was determined as 38.4 μm, the midpoint of the logarithmic size range. $N'(D_0)$ is the differential number concentration at D_0 (units of m^{-3} μm^{-1}). The non-dimensional ξ is the PSD slope, or Junge exponent, and ω is a correction parameter (dimensionless) of the power-law model that varies among different stations. Calculations were done using the least-squares minimization on the log-transformed data of each sample, as performed in previous studies [2,34]. Then, the two PSD slopes (ξ) and the correction parameter (ω) were derived. The spatial variability of these parameters for the surface waters of the study region was analyzed in this study. An important point to mention is that we defined surface waters as the average value of the layer between 0 and 2 m because in practice, it was difficult to observe the water information just beneath the surface (i.e., 0^-) due to the influence of strong waves in the study area, which is a semi-enclosed shallow sea.

In addition to mathematical models, percentile statistics are another way to describe and characterize size distributions of aquatic particles and can be calculated from the various measures of particle size, such as volume, number, and projected-area [2]. This study calculated the median particle diameter of the volume distribution, $D_v{}^{50}$, which corresponds to the 50th percentile diameter with half of an accumulated volume concentration. The parameter of $D_v{}^{50}$ carries information on the relative concentration of small to large particles at each station. The greater is the $D_v{}^{50}$, the greater is the dominance of the large particles, and vice versa.

2.4. Auxiliary Description

The LISST measurements provided particulate concentrations for each size class within a whole size spectrum of 2.5–500 μm, in terms of both volume and number. One way to show the variability in particle concentrations among samples is to use a particle concentration at a discrete size (such as N(D), where D = 37 μm) [34]. However, this only refers to a particle distribution at a specific size and does not contain information for all the other sizes. The present study used the total volume and number concentrations, V(D) and N(D), to represent the magnitude of the variability in particle concentrations, which were calculated by summing the quantities of all the size bins.

Statistical analysis was performed for several parameters, such as the particle volume and number concentrations, PSD slopes, and median particle diameters. The statistics included the minimum, maximum, mean, standard deviation (SD), and coefficient of variation (CV). A regression analysis was used to show the relationships between different bio-optical quantities. In addition, the residuals of

the power-law models were calculated to verify whether significant deviations occurred between the observed and modeled data, and the MAPE (Mean Absolute Percent Error) was defined as:

$$MAPE = \frac{1}{n}\sum_{i=1}^{n}\left|\frac{y_i' - y_i}{y_i}\right| \times 100\% \quad (5)$$

where, n is the number of samples; and y_i and y_i' represent the measured and modeled values, respectively.

3. Results

3.1. An Estimation of the PSD Slope Using the Power-Law Model

Power-law models with and without the correction parameters are both used to estimate the PSD slopes. Based on Equation (2), the model was generated by the regression analysis between $N'(D)/N'(D_0)$ and D/D_0.

Figure 2 shows two examples (Stations H5 and I1, which are selected randomly to represent the majority of the samples) of the performance of the model. For the two stations, the power-law model without the correction of the parameters (blue lines) performed better for medium-sized particles, while the power-law model with the correction of the parameters performed better for other particle sizes. A method was generated by combing the two models so that the power-law model without the correction of the parameters is used to describe the medium-sized particles, and the power-law model with the correction of the parameters is used for the smaller and larger particles. The MAPE values of the two models from all stations showed the same results (Figure 2b). Thus, a combined power-law model was used to describe the PSD slope for the study region. In this model, a particle size in the range of 16.8–87.9 μm was modeled using the power-law function without the correction of parameters, while for other sizes, the PSD slope was modeled using the same power law function with correction of the parameters. It is important to note that the slope parameters determined from the two individual models are very similar (mean absolute differences of 0.02 and mean relative difference of 1.5% for the slope range of 2.7–4.5, N = 79), and therefore, the PSD slope determined from the power-law model with the correction of the parameters was used in this study to describe the PSD in space and time.

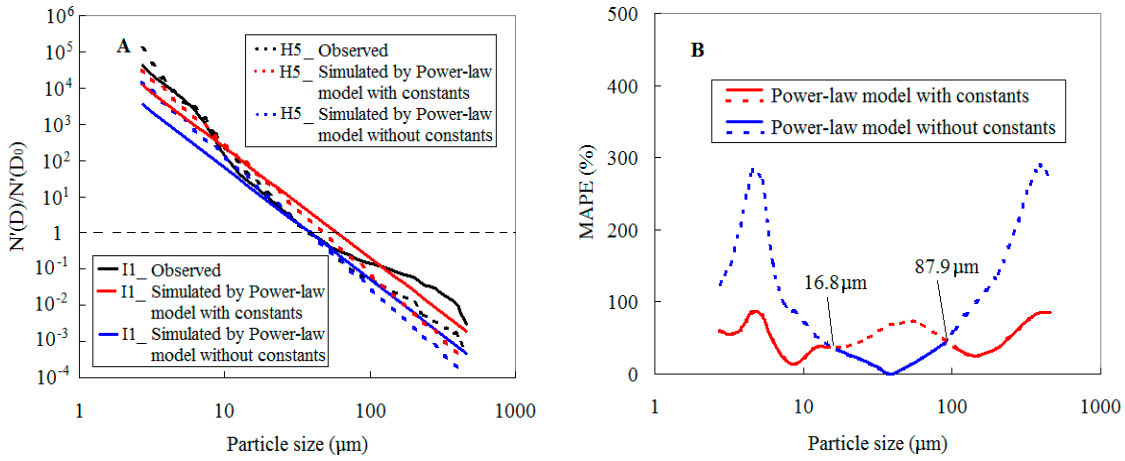

Figure 2. (**A**) The modeling performance of PSD at two typical stations (H5 and I1) using two power-law models (i.e., without/with correction of parameters), where the dotted lines and solid lines represent the correction of the model's independent (particle size or D/D_0) and dependent ($N'(D)/N'(D_0)$) variables at stations H5 and I1, respectively, and the colors black, red and blue represent the results of observation data, by using the power-law model with constants and without constants, respectively. (**B**) Errors (MAPE, %) in the modeled PSD for all stations (n = 79) in the whole particle size range.

3.2. The PSD and Bio-Optical Variability

Figure 3 shows the variability in the PSD parameters and the bio-optical parameters, including V(D) (in μL/L), N(D) (in 1 × 10^{10} count/m^3), $D_v{}^{50}$ (in μm), PSD slopes, and c_p (in m^{-1}), from the cruise (n = 79) in the Bohai and Yellow Seas in November 2013. V(D) varied 57-fold, ranging from 2.4 to 135.7 μL/L, with a mean of 26.0 ± 24.9 μL/L, and most (~70%) in the range of 5–35 μL/L. N(D) also showed relatively large variability, ranging from 0.3 to 58.2 (1 × 10^{10} count/m^3) with its CV of 112.3% and most samples (~73%) in the range of 0–15 (1 × 10^{10} count/m^3). The median particle diameter (50th percentile) of the volume distribution, $D_v{}^{50}$, ranged from 22.4 to 307.0 μm, with a non-normal distribution (Figure 3C). The particulate beam attenuation coefficient, c_p, varied between 4.2 and 24.4 m^{-1}, with a mean of 10.4 ± 3.8 m^{-1} and a Gaussian distribution with a relatively small CV (36.4%). Similarly, the PSD slope also showed large variations (Figure 3E).

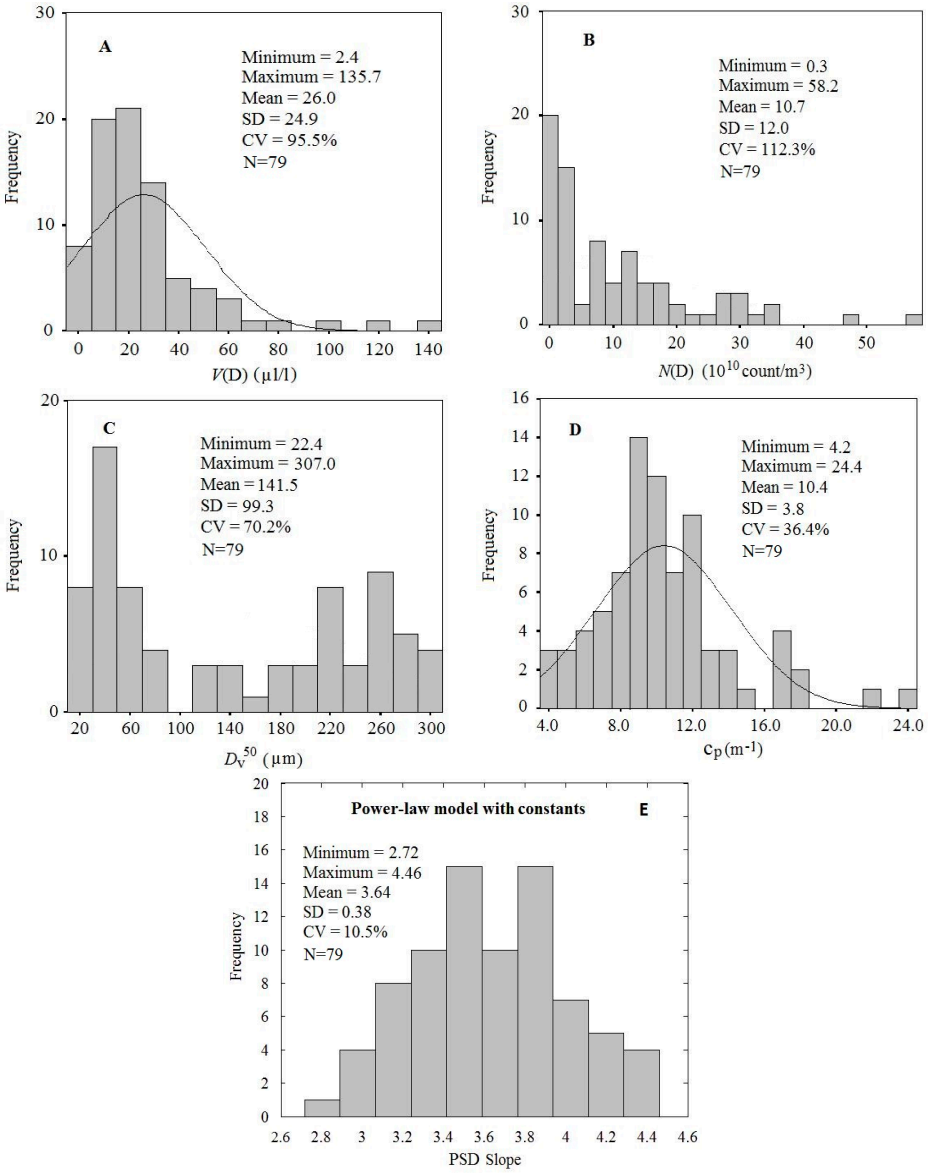

Figure 3. The variability in the bio-optical properties: (**A**) V(D) in μL/L; (**B**) N(D) in 1 × 10^{10} count/m^3; (**C**) $D_v{}^{50}$ in μm; (**D**) c_p in m^{-1} at a wavelength of 670 nm; and (**E**) PSD slope determined from the modified power-low model) in the Bohai Sea and the Yellow Sea, measured during the cruise (n = 79) in November 2013. SD: standard deviation; CV: coefficient of variation.

Figure 4 shows the relationships between the PSD parameters and the bio-optical properties measured at the 79 stations. Both V(D) and N(D) showed tight relationships with c_p, with their corresponding determination coefficients (R^2) being 0.815 ($p < 0.001$) and 0.681 ($p < 0.001$), respectively. Clearly, most of the variability in c_p can be explained by the particle concentration (in either volume or number). This is consistent with the prior knowledge, that is, the particle concentration is the first-order influencing factor for variation of inherent optical properties (IOPs) of particles, while other characteristics, such as size, composition, density, refraction, shape, may account for the second-order effect of IOPs' variation. D_v^{50} showed a weak (but still significant) negative correlation with c_p ($R^2 = 0.285$, $p < 0.001$), implying that large particles tend to attenuate light less. Finally, V(D) and N(D) are highly correlated ($R^2 = 0.778$, $p < 0.001$), suggesting that they may be equivalent when used to describe PSDs.

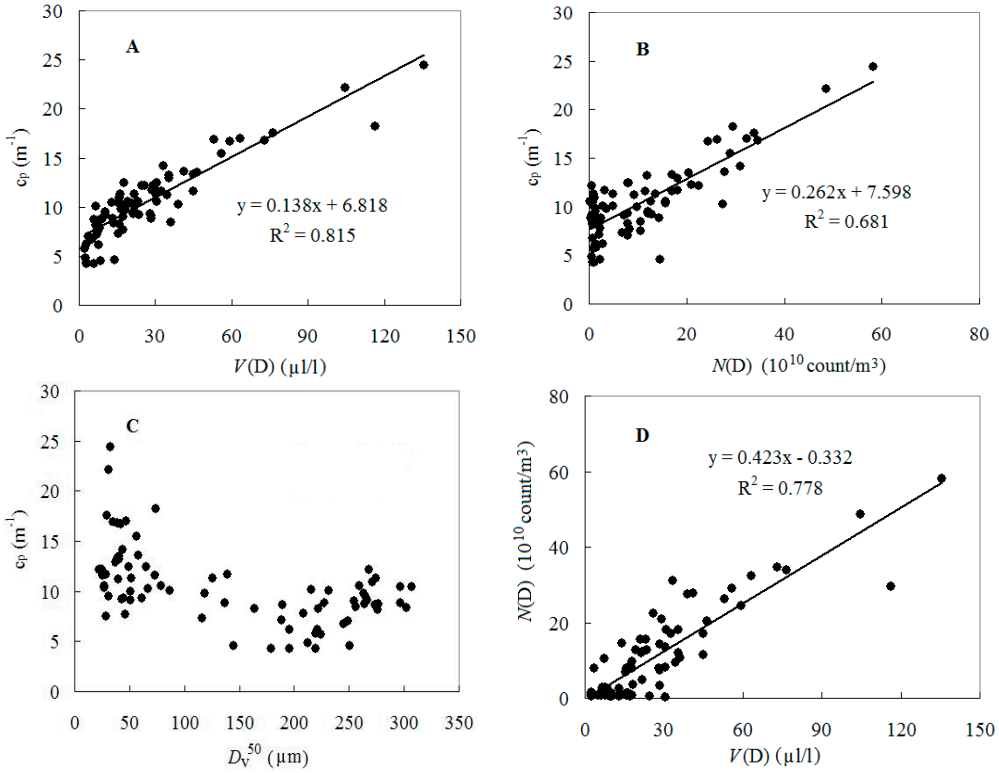

Figure 4. The relationships between the PSD parameters and the bio-optical properties in the Bohai Sea and the Yellow Sea, measured in November 2013 (n = 79): (**A**) V(D) vs. c_p; (**B**) N(D) vs. c_p; (**C**) D_v^{50} vs. c_p; and (**D**) V(D) vs. N(D).

3.3. Spatial Variability in PSD in Surface Waters

Figure 5 shows the spatial distribution of the PSD slopes and D_v^{50} determined from surface water measurements at the 79 stations in November 2013. The PSD slopes in the BS showed relatively high values (>3.8 for most waters). In the NYS, most waters away from the land had low PSD slopes (<3.4), while the near-land waters showed relatively high PSD slopes (~4.0). In the SYS, the PSD slopes in the northern part (~3.4) were generally lower than those in the southern part (>3.8); however the lowest values (<3.2) were found in the center of the SYS.

D_v^{50} showed opposite spatial distribution patterns relative to the PSD slopes (Figure 5B). Indeed, there existed a significant negative relationship between the two parameters ($R^2 = 0.744$, $p < 0.001$, Figure 5C), suggesting that the PSD slopes also contain information on the relative proportions of different particle sizes. The results obtained by this study confirmed the fact that the PSD slopes carry information on the relative concentrations of small to large particles, namely the greater the

slopes the less proportion of large particles, and the smaller the slopes the more proportion of large particles. This observation is consistent with findings reported by Buonassissi and Dierssen (2010) [34]. In addition, another parameter, namely the correction parameter in the power-law model, generally showed a positive relationship with the $D_v{}^{50}$ ($R^2 = 0.691$, $p < 0.01$) (figure not shown). This indicates that the more large particles the greater the correction parameter, and vice versa.

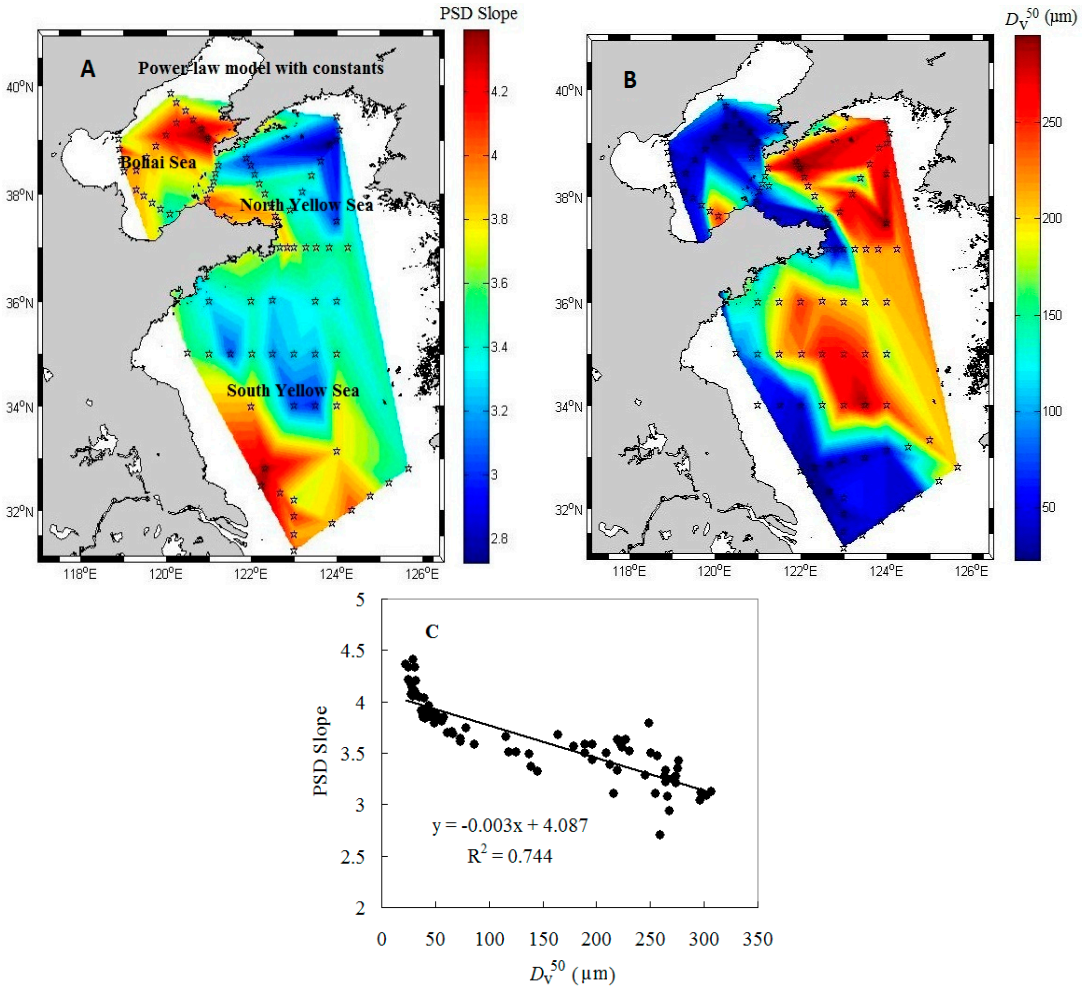

Figure 5. The spatial distribution of: (**A**) the PSD slopes; and (**B**) $D_v{}^{50}$ in surface waters of the Bohai Sea and Yellow Sea in November 2013 (n = 79); and the relationship between the two parameters (**C**).

3.4. Vertical Variability in PSD

For the three pre-defined layers (upper layer: 0–5 m; middle layer: 5–20 m; and deep layer: 20–90 m), Figure 6 shows the statistics of the PSD slopes, with a slightly decreasing trend from the surface layer (3.79) to the bottom layer (3.69). This decrease indicates that relatively small particles dominate the upper layer while larger particles dominate the bottom layer, a possible result of precipitation. These results are presented differently in Figure 7, where the data were binned to 5-m intervals, and the means and standard deviations for the PSD slopes were calculated for each bin. When data from all the stations were combined, the mean PSD slopes showed a decreasing trend from the surface to a depth of 25 m, and then gradually increased until water depth reached 50 m, and then decreased again when approaching the bottom. Such distributions varied from region to region. Mean PSD slopes in the BS were higher than those in the NYS, although they both decreased from the surface to the bottom (Figure 7B,C). This PSD indicates the presence of more small particles in the BS than in the NYS. Although in all the regions there appeared to be an intermediate layer between

30 and 60 m with relatively high PSD slopes, this trend was more apparent in the SYS. The SYS showed generally larger PSD slopes than the NYS, indicating relatively more small particles in the SYS than in the NYS.

Interestingly, note that there were large values of PSD slopes at the bottom compared to the surface in Bohai Sea, as shown in Figure 7B. This may be potentially related to its geophysical and hydrologic characteristics. As the largest inner sea of China, the BS covers Yellow River (the largest river of China) estuary, and is strongly influenced by surrounding numerous rivers, well-known for a large amount of suspended sediment discharge [64,65]. The sediments with sizes of 10–25 μm contributed most of the materials that inputted into the BS, promoting Yellow River delta epeirogeny, when large-sized sediments (>25 μm) had less contribution and more easily deposited in the river course [66]. However, the suspended particles in the surface water column are easily dominated by large-sized algae, such as diatom (>20 μm). Hence, fine inorganic particles may explain the large PSD slope at the bottom when large algal particles are corresponding to the relatively low slopes at the surface water column.

As shown in Figure 7D, the PSD slope showed large values between 30 and 60 m depth, which is possibly related to the halocline, chlorophyll maxima depth, and hydrography. However, it is unfortunate that these related materials are not available in this cruise. Even so, Zou et al. (2001) had reported that the halocline in SYS was about between 30 and 60 m depth by using the samples from November 1997, which is consistent with the sampling month of this study [67]. Fu et al. (2009) demonstrated that the chlorophyll maxima depth also varied near to this depth range (see Figure 5 in that paper) [68]. More detailed reasons for this phenomenon in the SYS should be addressed through more complete and synchronous materials in the future.

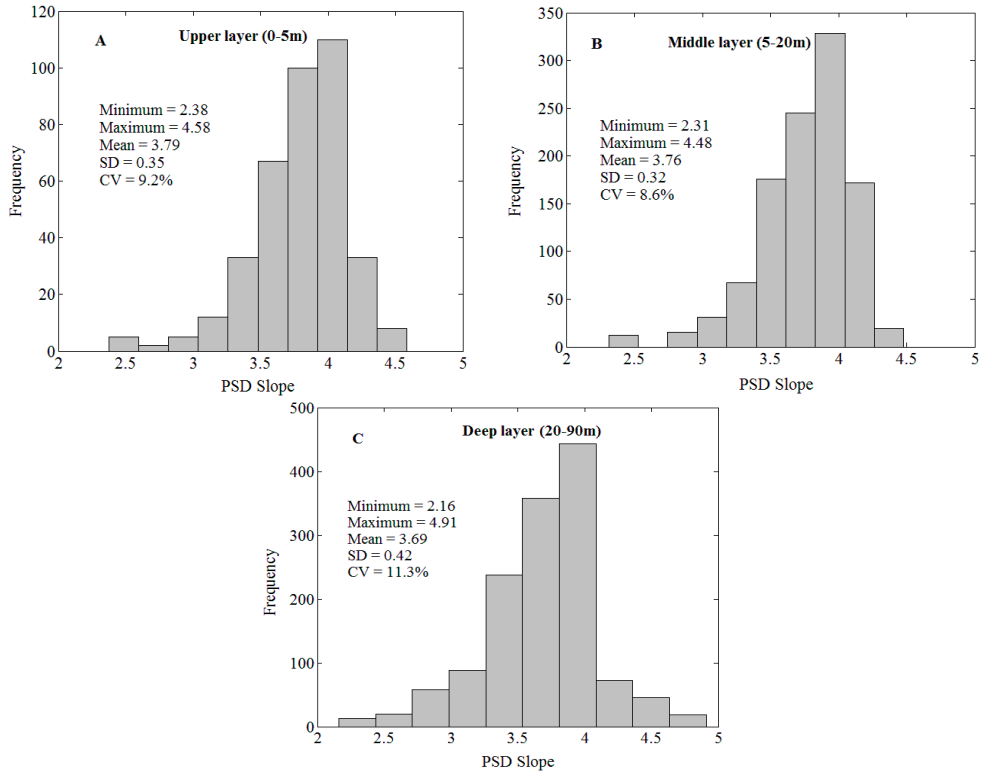

Figure 6. The statistics of the PSD slopes in the: (**A**) upper layer (0–5 m) (n = 375); (**B**) middle layer (5–20 m) (n = 1065); and (**C**) deep layer (20–90 m) (n = 1354) of the water column. These sample numbers were determined by LISST sampling frequency (1 count·s^{-1}) and residence time during the observation period in each specific layer, which is the time required for the LISST to travel down through the upper layer (0–5 m), middle layer (5–20 m), and deep layer (20–90 m).

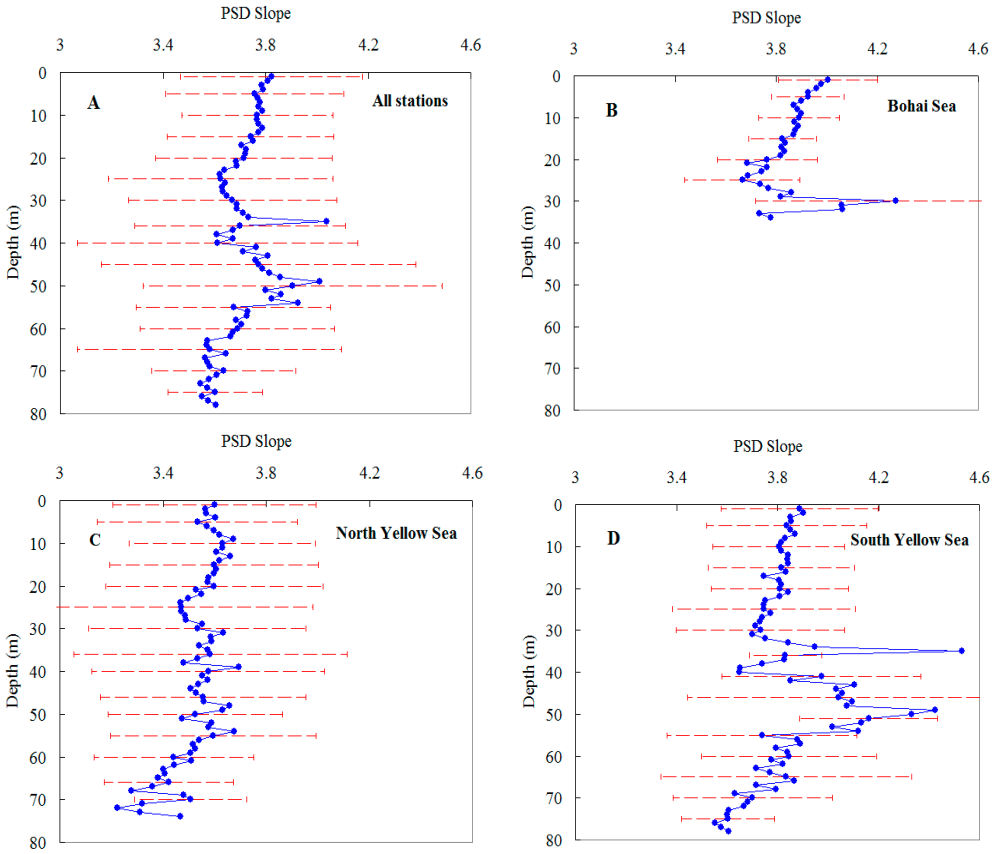

Figure 7. The vertical profiles of the mean and the standard deviation (SD) of the PSD slopes at 5 m intervals: (**A**) all stations (n = 79); (**B**) Bohai Sea (n = 20); (**C**) North Yellow Sea (n = 29); and (**D**) South Yellow Sea (n = 30). Note that the Bohai Sea is relatively shallow, and the profiles were limited to the first 40 m.

To further illustrate the vertical variability in the PSDs, three stations were selected as representatives of the various water environments (Figures 8 and 9), i.e., M4, J4, and A5. These stations are located in the central regions of the BS, NYS, and SYS, respectively, with different water depths. For M4 (water depth = 20 m), N(D) and V(D) did not show apparent vertical trends, although some fluctuations were found at different water depths. The PSD slopes showed similar fluctuation patterns as N(D), ranging between 3.83 and 3.98 (mean = 3.91, SD = 0.05). Relatively stable c_p(670) was observed (9.1–9.8 m^{-1}, mean = 9.4 m^{-1} and SD = 0.2 m^{-1}) but c_p(670) showed a tight statistical relationship with N(D) (R^2 = 0.646, $p < 0.001$) (Figure 9A). For J4 (water depth = 65 m), both N(D) and V(D) were stable for the upper 30 m (N(D) ~2.5 × 10^{10} count/m^3; V(D) ~20 μL/L), and then gradually increased to the bottom. Both the PSD slopes and c_p(670) showed relatively large ranges (~1.0 and 8.4–10.0 m^{-1}, respectively), and c_p(670) also showed an increasing trend from the surface to the bottom, similarly to the N(D) and V(D) profiles (Figure 8G,H). At this location, c_p(670) showed close relationships with both N(D) and V(D) (Figure 9C). For A5 (water depth = 47 m), the PSD slopes showed a slightly decreasing pattern from the surface to the bottom (3.90 to 3.70). c_p(670) was approximately 10 m^{-1} for the surface (0–30 m) waters and then rapidly increased to the bottom. Similarly to other stations, c_p(670) showed tight relationships with both N(D) (R^2 = 0.951, $p < 0.001$) and V(D) (R^2 = 0.918, $p < 0.001$) (Figure 9E). Overall, particle concentrations showed tight relationships with c_p(670), but the PSD slopes were not usually significantly correlated with c_p(670) (as in Figure 9B,D,F). Additionally, it is worth noting that there are high volume concentrations of suspended particles in lower size classes in the BS compared with the NYS and the SYS (Figure 8B,E,J). This is closely linked with high content of small-sized sediments discharged by surrounding numerous rivers along the BS, which is an approximately closed

inner sea. For instance, the largest river (Yellow River) of China discharged a total annual run-off of 8.88 × 10^{10} m^3 into the BS [69], where large particles easily accumulated on the riverbed while small-sized sediments flowed into the BS [66]. In contrast, the YS is more open than the BS, and possibly influenced by terrigenous runoff at a less degree than the BS.

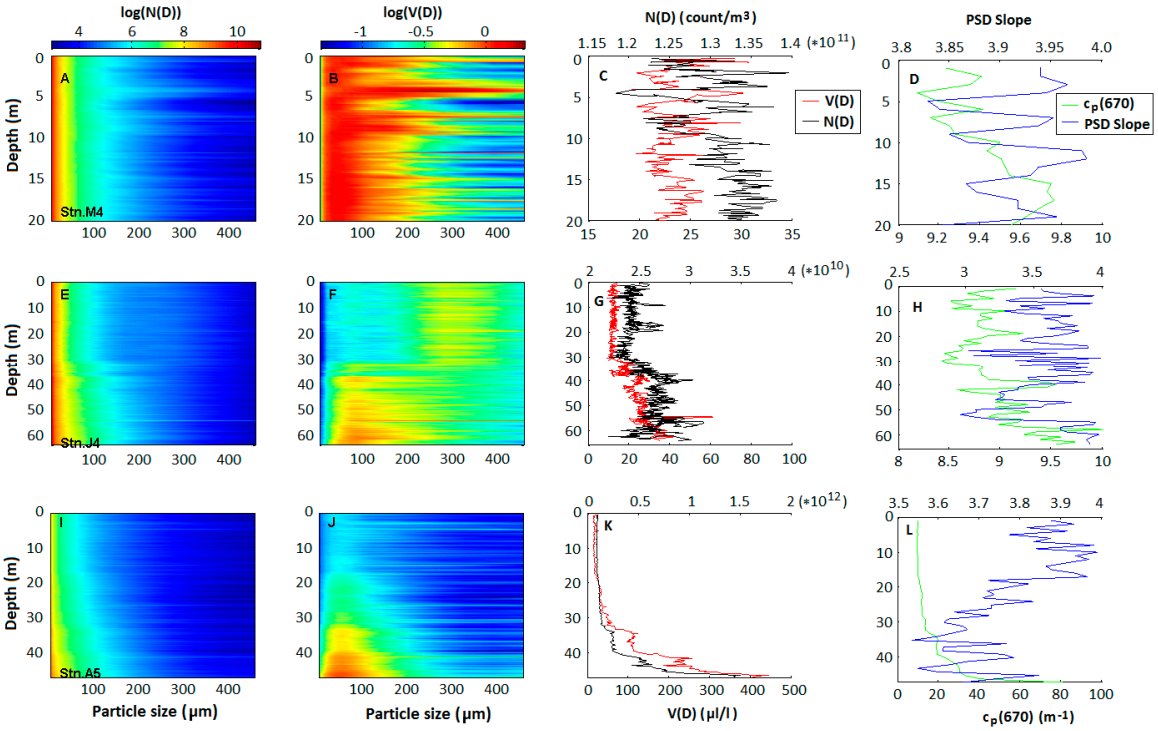

Figure 8. (**A**–**L**) The vertical distributions of the size-specific particle numbers and volume concentrations for each of the size bins (**left two columns**), total particle number and volume concentrations (**the third column**), and PSD slopes and $c_p(670)$ (**last column**) from three representative stations located in the BS ((**top**) Stn. M4, Stn means Station), NYS ((**middle**) Stn. J4), and SYS ((**bottom**) Stn. A5), respectively.

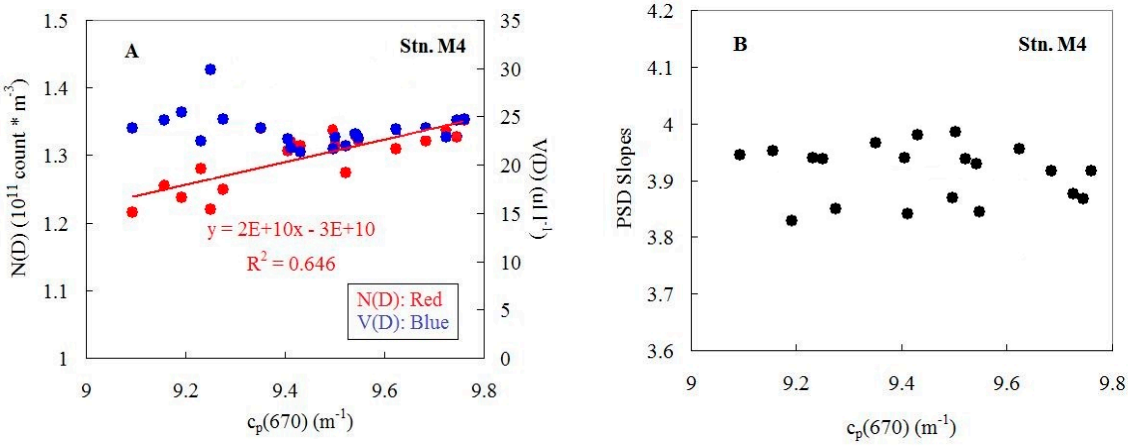

Figure 9. *Cont.*

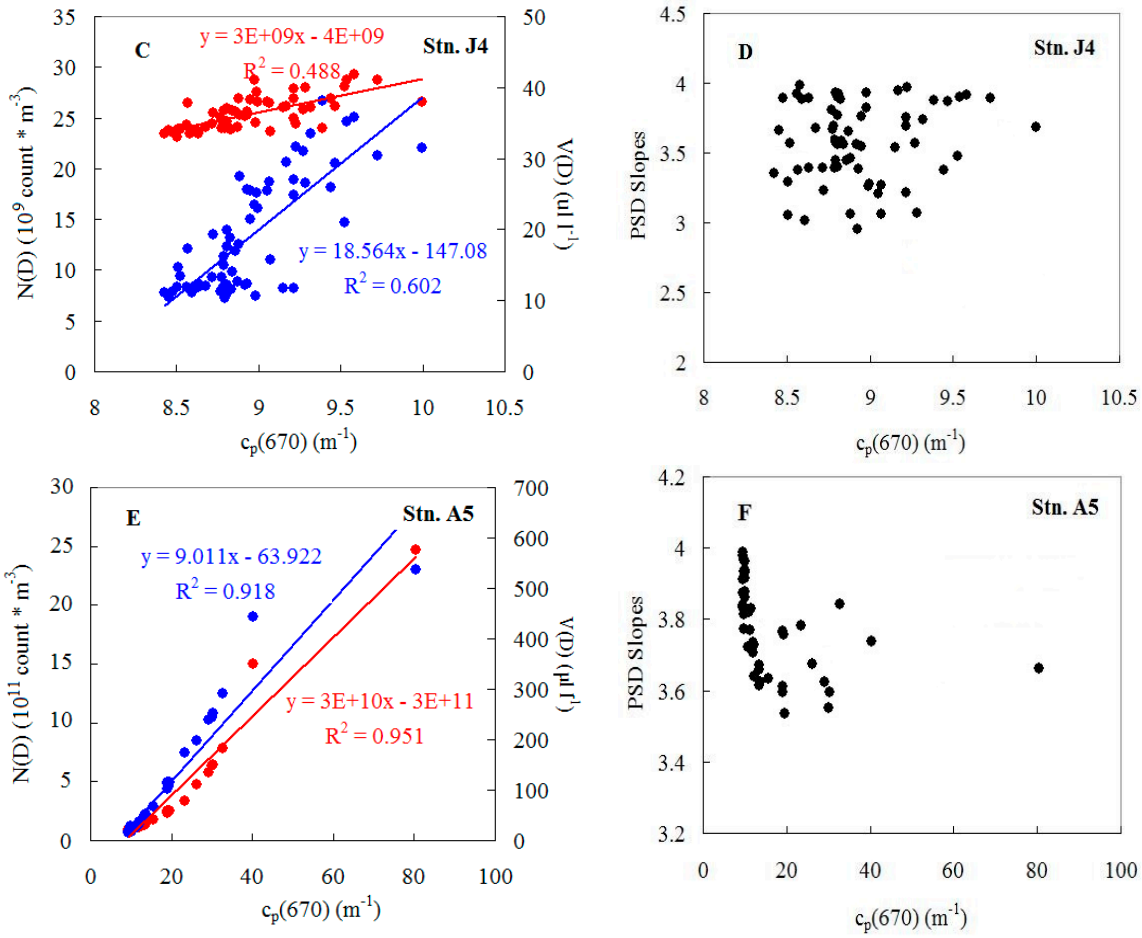

Figure 9. (**A**–**F**) The statistical relationships between the different PSD and the bio-optical parameters obtained at different water depths from the three representative stations (M4, J4, and A5 in the BS, NYS, and SYS, respectively).

4. Discussion

With the increased use of the LISST instrument in recent years, the PSD slopes from different marine waters have been reported by a number of studies. Several representative results are listed in Table 1 to provide a context and a comparison of the results presented in this study. Of these, Buonassissi and Dierssen (2010) reported a range of 2.7–4.7 (mean = 3.63) from 175 stations along the east and west coasts of America and the Atlantic sector of the Southern Ocean [34], and Neukermans et al. (2012) reported a range of 2.5–4.5 from 366 stations in coastal and offshore waters around Europe and French Guyana [11]. Lower values of approximately 2.0 were reported by Reynolds et al. (2010) for European coastal waters [2]. In the present study, the PSD slopes obtained in the BS and the YS varied from 2.72 to 4.46, which was well in line with previously reported ranges. It is important to note that the mean PSD slopes from previous studies from different regions were stable (3.4 or 3.6) (Table 1), suggesting similarity in the overall PSDs in these different waters.

In this study, although the surface PSDs showed some differences between the three different regions (BS, NYS, and SYS), they all showed a predominance of smaller particles in nearshore waters, where terrestrial inorganic sediments contributed significantly to total suspended matter. In the offshore waters of these regions, lower PSD slopes were possible indicators of large-sized phytoplankton. Small particles are generally mineral particles with a high refraction index, while larger particles are biological in origin with a lower refraction index [70]. The observations in this study are in line with those reported by Xi et al. (2014) for the Hudson Bay [4].

Table 1. Variations of PSD slopes reported in the published literature and in this study.

Water Regions	Ranges of PSD Slopes	Mean (± SD)	Stations	References
The east and west coast of America and the Atlantic sector of the Southern Ocean	2.7–4.7	3.63	175	Buonassissi and Dierssen, 2010 [34]
Coastal and offshore waters around European and French Guyana	2.5–4.5	Case 1 water: 3.4 (±0.3); Case 2 water: 3.4 (±0.4)	366	Neukermans et al., 2012 [11]
The global oceans	3.04–5.99 (Satellite retrieval)	4.22 (±0.59)	480,231	Kostadinov et al., 2009 [1]
European coastal waters	2.0–4.0	3.47	36	Reynolds et al., 2010 [2]
Monterey Bay	2.5–4.3	3.46	14	Reynolds et al., 2010 [2]
Hudson Bay	2.84–4.46	3.63 (±0.40)	33	Xi et al., 2014 [4]
Bohai Sea and Yellow Sea	2.72–4.46	3.64 (±0.38)	79	This study

In addition to being the first report of PSD variability in these three regions, this study also used an empirical power-law model to describe the PSD. This model is actually a combination of an original power-law model fitted for the medium-sized particles and a modified power-law model for other sizes, and still belongs to common practice, i.e., power-law function fitting. As an independent validation, Figure 10 demonstrated the good performance of the combined model, by using the in situ dataset (n = 75) collected from the Bohai Sea and Yellow Sea in November 2014. It means that the combined model used in this study is capable to capture the PSD characteristics, at least in the study areas. However, it is necessary to note that the power-law model could not be well used to describe the PSD for the entire size range, as found in previous studies [4,29,30,34]. This study also indicates that the selection of the reference particle size might potentially influence the PSD slopes derived from the power-law model (data no shown). Indeed, researches on best estimations of PSD slopes have been performed for different reference sizes, such as 1 μm [34], 2 μm [1], and 37.6 μm [4], and different size ranges, such as 4.5–10 μm, 4.5–104 μm, and 4.5–280 μm [71,72]. In this study, we investigated the PSD spatial distribution of the study area based on in situ laser diffraction measurements during November 2013. Note that the observation stations were actually investigated on different dates and time during a month, and so some factors such as tidal current, waves and turbulence [25–28], might show a certain impact on temporal variability of PSD. However, it is very difficult to do synchronous observation on all these stations in the investigated water areas, which limits the plot of spatial distribution in a rigorously simultaneous manner. Instead, Figure 5A,B could show the spatial distribution characteristic at least on a monthly-time scale. A long-term mooring buoy observation is expected in future to investigate the influence of tide, turbulence, currents, and wind to PSD. In addition, the temporal variability is another important aspect for investigating PSD characteristics, and should be studied in the future when sufficient datasets would be collected in different seasons, and even different years.

Remote sensing technology provides a powerful tool for detecting the large-scale PSD information. A commonly used method for the PSD retrievals is through "Junge distribution" model [2,9,34], referred as the default power-law model. In this study, the PSD model has been updated with combining the default power-law model and a modified power-law model with a correction parameter for different particle size ranges. The new model, which performed more accurate simulation for the PSD than the default power-law model, will potentially improve remote sensing retrievals of the PSD, at least in the research areas. One key parameter used in remote sensing algorithms is the PSD slope, ξ, which can link the PSD with the spectral slope (η) of particle backscattering or attenuation coefficients by the equation of $\xi \approx \eta + 3$ or other correction relationships [1,9,10]. Using SeaWiFS global data from August 2007 and a remote sensing algorithm to retrieve PSD slopes, Kostadinov et al. (2009) showed global distributions ranging from 3.04 to 5.99 [1]. In this study the PSD slopes obtained in the BS and

the YS varied from 2.72 to 4.46, which was consistent with the remote sensing retrievals provided by Kostadinov et al. (2009) [1]. Another important quantity for the remote sensing retrievals of the PSD is the correction parameter in the new model, ω. It was found to be closely related with the D_v^{50} ($R^2 = 0.691$, $p < 0.01$), and would in general increase along with the increase of the median diameter and vice versa, which implied that the power-law model might need more correction by using greater coefficients when large particles appeared in some stations. Obviously, it would be further linked to mass-specific backscattering or attenuation. In addition, previous studies have shown the influence of suspended particle size distribution on optical properties and remote sensing reflectance [73,74]. Thus, a potential remote sensing retrieval for the PSD based on the new model will be helpful to precisely estimate the water properties from satellite remote sensing. How to establish a remote sensing algorithm to estimate PSD is beyond the scope of this study, and will be possibly elaborated in detail in future research. Furthermore, similar to the PSD, the bulk refractive index is also essential to describe the characteristics of suspended particles. It is worth noting that a new remote sensing model has been developed to retrieve the refractive index in recent studies [75,76].

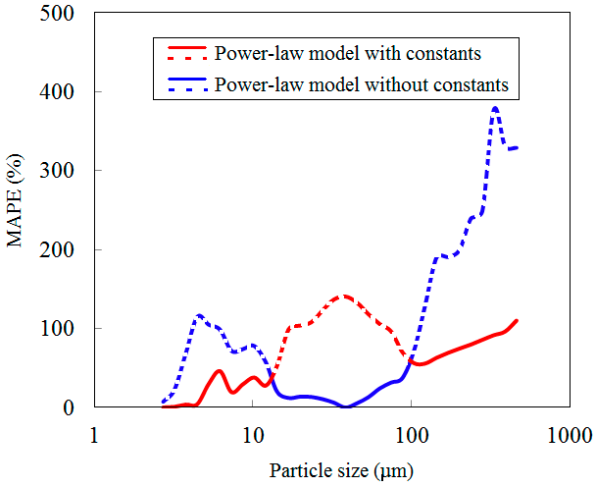

Figure 10. A comparison of MAPE (%) derived from the power-law models with/without constants, by using an independent validation dataset (n = 75) collected from the Bohai Sea and the Yellow Sea in November 2014.

5. Conclusions

In this study, we investigate the PSD properties and variability in two typical shallow and semi-enclosed seas of China, Bohai Sea and Yellow Sea, based on in situ laser diffraction measurements (LISST-100X Type C) and other measurements during November 2013. Large variations were found in particle concentrations from LISST measurements. The volume concentrations varied by 57 folds. The median particle diameter (D_v^{50}) from each of the water samples also covers a large range (22.4–307.0 μm) and shows an irregular statistical distribution.

Power-law models with and without the correction parameters were used to evaluate PSD. Large variations were also found in PSD in the Bohai Sea and Yellow Sea, with higher slopes in near-shore surface waters than in offshore surface waters. Significant regional and vertical variability in the PSD indicated the complexity of suspended particulate composition in our investigated water regions. These results are consistent with the general knowledge that near shore waters are under more influence of small particles of terrestrial origin.

To conclude, this study provides fundamental knowledge on particle size properties, and documents variability of the PSD as a key parameter describing the nature of suspended assemblages in Bohai Sea and Yellow Sea waters. The generation of the PSD model of this study provides a potential help to precisely estimate the water properties from satellite remote sensing. Further study should

focus on the improvement in the remote sensing algorithms for PSD estimation, seasonal variability of the PSD by extending PSD observations, and comprehensively characterizing the PSD based on more cruise datasets. In addition, it is an important and interesting subject for water optics and remote sensing to study how the spatial and temporal changes of PSD influence on optical properties of marine particles in Bohai Sea and Yellow Sea waters and remote sensing algorithms for estimating particle concentrations and sizes.

Acknowledgments: This research was jointly supported by the National Natural Science Foundation of China (No. 41276186, 41576172, and 41506200), the National Key Research and Development Program of China (No. 2016YFC1400901 and 2016YFC1400904), the Provincial Natural Science Foundation of Jiangsu in China (No. BK20151526 and BK20150914), the Natural Science Foundation of the Jiangsu Higher Education Institutions of China (No. 15KJB170015), sponsored by Qing Lan Project, the National Program on Global Change and Air-sea Interaction (No. GASI-03-03-01-01), the Public Science and Technology Research Funds Projects of Ocean (201005030), and a project funded by "the Priority Academic Program Development of Jiangsu Higher Education Institutions (PAPD)". We acknowledge the important contribution of Shuguo Chen who provided a great help in the field investigation, and the works of Yibo Yuan, Xiaojing Shen, Yahui Chen, Hailong Zhang, and Cong Xiao.

Author Contributions: Zhongfeng Qiu designed this study and the algorithm; Deyong Sun contributed to the data analyses and drafted the manuscript; Chuanmin Hu contributed to the improvement of the paper quality; ShengqiangWang, and Lufei Zheng assisted with developing the research design and results interpretation; Yu Huan and Tian Peng contributed to the interpretation of results and manuscript revision.

Conflicts of Interest: The authors declare no conflict of interest.

References

1. Kostadinov, T.S.; Siegel, D.A.; Maritorena, S. Retrieval of the particle size distribution from satellite ocean color observations. *J. Geophys. Res.* **2009**. [CrossRef]
2. Reynolds, R.A.; Stramski, D.; Wright, V.M.; Woźniak, S.B. Measurements and characterization of particle size distributions in coastal waters. *J. Geophys. Res.* **2010**. [CrossRef]
3. Bader, H. The hyperbolic distribution of particle sizes. *J. Geophys. Res.* **1970**, *75*, 2822–2830. [CrossRef]
4. Xi, H.; Larouche, P.; Tang, S.; Michel, C. Characterization and variability of particle size distributions in Hudson Bay. *Can. J. Geophys. Res. Oceans* **2014**, *119*, 3392–3406. [CrossRef]
5. Falkowski, P.G.; Barber, R.T.; Smetacek, V. Biogeochemical controls and feedbacks on ocean primary production. *Science* **1998**, *281*, 200–206. [CrossRef] [PubMed]
6. Le Quéré, C.; Harrison, S.P.; Prentice, I.C.; Buitenhuis, E.T.; Laurent Bopp, O.A.; Claustre, H.; Da Cunha, L.C.; Geider, R.; Giraud, X.; Klaas, C.; et al. Ecosystem dynamics based on plankton functional types for global ocean biogeochemistry models. *Glob. Chang. Biol.* **2005**, *11*, 2016–2040.
7. Boss, E.; Pegau, W.S. The relationship of light scattering at an angle in the backward direction to the backscattering coefficient. *Appl. Opt.* **2001**, *40*, 5503–5507. [CrossRef] [PubMed]
8. Boss, E.; Pegau, W.S.; Gardner, W.D.; Zaneveld, R.V.; Barnard, A.H.; Twardowski, M.S.; Chang, G.C.; Dickey, T.D. Spectral particulate attenuation and particle size distribution in the bottom boundary layer of a continental shelf. *J. Geophys. Res.* **2001**, *106*, 9509–9516. [CrossRef]
9. Boss, E.; Twardowski, M.S.; Herring, S. Shape of the particulate beam attenuation spectrum and its inversion to obtain the shape of the particulate size distribution. *Appl. Opt.* **2001**, *40*, 4885–4893. [CrossRef] [PubMed]
10. Twardowski, M.S.; Boss, E.; MacDonald, J.B.; Pegau, W.S.; Barnard, A.H.; Zaneveld, J.R.V. A model for estimating bulk refractive index from optical backscattering ratio and the implications for understanding particle composition in case I and case II waters. *J. Geophys. Res.* **2001**. [CrossRef]
11. Neukermans, G.; Loisel, H.; Mériaux, X.; Astoreca, R.; McKee, D. In situ variability of mass-specific beam attenuation and backscattering of marine particles with respect to particle size, density, and composition. *Limnol. Oceanogr.* **2012**, *1*, 124–144. [CrossRef]
12. Ahn, J.H. Size distribution and settling velocities of suspended particles in a tidal embayment. *Water Res.* **2012**. [CrossRef] [PubMed]
13. Buesseler, K.O.; Lamborg, C.H.; Boyd, P.W.; Lam, P.J.; Trull, T.W.; Bidigare, R.R.; Bishop, J.K.B.; Casciotti, K.L.; Dehairs, F.; Elskens, M.; et al. Revisiting carbon flux through the ocean's twilight zone. *Science* **2007**, *316*, 567–570. [CrossRef] [PubMed]

14. Mikkelsen, O.; Pejrup, M. The use of a LISST-100 laser particle sizer for in-situ estimates of floc size, density and settling velocity. *Geo-Mar. Lett.* **2001**, *20*, 187–195. [CrossRef]
15. Carder, K.L.; Costello, D.K. Optical effects of large particles. In *Ocean Optics*; Spinrad, R.W., Carder, K.L., Perry, M.J., Eds.; Oxford University Press: Oxford, UK, 1994; pp. 243–257.
16. Jonasz, M.; Fournier, G. *Light Scattering by Particles in Water: Theoretical and Experimental Foundations*; Academic Press: London, UK, 2007.
17. Stramski, D.; Boss, E.; Bogucki, D.; Voss, K.J. The role of seawater constituents in light backscattering in the ocean. *Prog. Oceanogr.* **2004**, *61*, 27–56. [CrossRef]
18. Stramski, D.; Woźniak, S.B. On the role of colloidal particles in light scattering in the ocean. *Limnol. Oceanogr.* **2004**, *50*, 1581–1591. [CrossRef]
19. Peng, F.; Effler, S.W.; O'Donnell, D.; Perkins, M.G.; Weidemann, A. Role of minerogenic particles in light scattering in lakes and a river in central New York. *Appl. Opt.* **2007**, *46*, 6577–6594. [CrossRef] [PubMed]
20. Jackson, G.A.; Maffione, R.; Costello, D.K.; Alldredge, A.L.; Logan, B.E.; Dam, H.G. Particle size spectra between 1 mm and 1 cm at Monterey Bay determined using multiple instruments. *Deep Sea Res.* **1997**, *44*, 1739–1767. [CrossRef]
21. Stemmann, L.; Eloire, D.; Sciandra, A.; Jackson, G.A.; Guidi, L.; Picheral, M.; Gorsky, G. Volume distribution for particles between 3.5 to 2000 mm in the upper 200 m region of the South Pacific Gyre. *Biogeosciences* **2008**, *5*, 299–310. [CrossRef]
22. Slade, W.; Boss, E. Calibrated near-forward volume scattering function obtained from the LISST particle sizer. *Opt. Express* **2006**, *8*, 3602–3615. [CrossRef]
23. Anglès, A.; Jordi, A.; Garcés, E.; Masó, M.; Basterretxea, G. High-resolution spatio-temporal distribution of a coastal phytoplankton bloom using laser in situ scattering and transmissometry (LISST). *Harmful Algae* **2008**, *7*, 808–816. [CrossRef]
24. Aurin, D.; Dierssen, H.M.; Twardowski, M.S.; Roesler, C.S. Optical complexity in Long Island Sound and implications for coastal ocean color remote sensing. *J. Geophys. Res.* **2010**. [CrossRef]
25. Renosh, P.R.; Schmitt, F.G.; Loisel, H.; Sentchev, A.; Mériaux, X. High frequency variability of particle size distribution and its dependency on turbulence over the sea bottom during re-suspension processes. *Cont. Shelf Res.* **2014**, *77*, 51–60. [CrossRef]
26. Renosh, P.R.; Schmitt, F.G.; Loisel, H. Intermittent particle dynamics in marine coastal waters. *Nonlinear Process. Geophys.* **2015**, *22*, 5, 633–643. [CrossRef]
27. Wolanski, E.; Gibbs, R.J. Flocculation of suspended sediment in the Fly River Estuary, Papua New Guinea. *J. Coast. Res.* **1995**, *11*, 754–762.
28. Velegrakis, A.F.; Michel, D.; Collins, M.B.; Lafite, R.; Oikonomou, E.K.; Dupont, J.P.; Bishop, C. Sources, sinks and resuspension of suspended particulate matter in the eastern English Channel. *Cont. Shelf Res.* **1999**, *19*, 1933–1957. [CrossRef]
29. Ceronio, A.D.; Haarhoff, J. An improvement on the power law for the description of particle size distributions in potable water treatment. *Water Res.* **2005**, *39*, 305–313. [CrossRef] [PubMed]
30. Ferry, S.; Zirlewagen, J.; Hillebrand, O.; Licha, T.; Scheytt, T. Preliminary results on the dynamics of particles and their size distribution at a Karst spring during a snowmelt event. *J. Hydrol.* **2015**, *524*, 326–332.
31. Jonasz, M. Nonspherical sediment particles: Comparison of size and volume distributions obtained with an optical and resistive particle counter. *Mar. Geol.* **1987**, *78*, 137–142. [CrossRef]
32. Kitchen, J.; Menzies, D.; Pak, H.; Zaneveld, J. Particle size distributions in a region of coastal upwelling analyzed by characteristic vectors. *Limnol. Oceanogr.* **1975**, *20*, 775–783. [CrossRef]
33. Risovic, D. Two-component model of sea particle size distribution. *Deep Sea Res.* **1993**, *40*, 1459–1473. [CrossRef]
34. Buonassissi, C.J.; Dierssen, H.M. A regional comparison of particle size distributions and the power law approximation in oceanic and estuarine surface waters. *J. Geophys. Res.* **2010**. [CrossRef]
35. Monahan, E.C.; Zietlow, C.R. Laboratory comparisons of fresh-water and salt-water whitecaps. *J. Geophys. Res.* **1969**, *28*, 6961–6966. [CrossRef]
36. Seibel, B.A. On the depth and scale of metabolic rate variation: Scaling of oxygen consumption rates and enzymatic activity in the class Cephalopoda (Mollusca). *J. Exp. Biol.* **2007**, *210*, 1–11. [CrossRef] [PubMed]
37. Sheldon, R.W.; Prakash, A.; Sutcliffe, W.H., Jr. The size distribution of particles in the ocean. *Limnol. Oceanogr.* **1972**, *17*, 327–340. [CrossRef]

38. Kiefer, D.A.; Berwald, J. A random encounter model for the microbial planktonic community. *Limnol. Oceanogr.* **1992**, *15*, 457–467. [CrossRef]
39. Karageorgis, A.P.; Georgopoulos, D.; Kanellopoulos, T.D.; Mikkelsen, O.A.; Pagou, K.; Kontoyiannis, H.; Paylidou, A.; Anagnostou, Ch. Spatial and seasonal variability of particulate matter optical and size properties in the Eastern Mediterranean Sea. *J. Mar. Syst.* **2012**, *12*, 123–134. [CrossRef]
40. Xi, H.; Larouche, P.; Michel, C.; Tang, S. Beam attenuation, scattering and backscattering of marine particles in relation to particle size distribution and composition in Hudson Bay (Canada). *J. Geophys. Res. Oceans* **2015**. [CrossRef]
41. Woźniak, S.B.; Stramski, D.; Stramska, M.; Reynolds, R.A.; Wright, V.M.; Miksic, E.Y.; Cichocka, M.; Cieplak, A.M. Optical variability of seawater in relation to particle concentration, composition, and size distribution in the nearshore marine environment at Imperial Beach, California. *J. Geophys. Res.* **2010**. [CrossRef]
42. Peng, F.; Effler, S.W. Mass-specific scattering coefficient for natural minerogenic particle populations: Particle size distribution effect and closure analyses. *Appl. Opt.* **2012**, *51*, 2236–2249. [CrossRef] [PubMed]
43. Wang, S.; Qiu, Z.; Sun, D.; Shen, X.; Zhang, H. Light beam attenuation and backscattering properties of particles in the Bohai Sea and Yellow Sea with relation to biogeochemical properties. *J. Geophys. Res. Oceans* **2016**. [CrossRef]
44. Sun, D.; Qiu, Z.; Hu, C.; Wang, S.; Wang, L.; Zheng, L.; Peng, T.; He, Y. A hybrid method to estimate suspended particle sizes from satellite measurements over Bohai Sea and Yellow Sea. *J. Geophys. Res. Oceans* **2016**. [CrossRef]
45. Morel, A.; Prieur, L. Analysis of variations in ocean color. *Limnol. Oceanogr.* **1977**, *22*, 709–722. [CrossRef]
46. Wei, H.; Sun, J.; Moll, A.; Zhao, L. Phytoplankton dynamics in the Bohai Sea—Observations and modeling. *J. Mar. Syst.* **2004**, *44*, 233–251. [CrossRef]
47. Feng, S.; Li, F.; Li, S. Atmosphere and ocean. In *Introduction of Marine Sciences*; Higher Education Press: Beijing, China, 1999; pp. 233–267.
48. He, Y.; Lu, X.; Qiu, Z.; Zhao, J. Shallow water tidal constituents in the Bohai Sea and the Yellow Sea from a numerical adjoint model with TOPEX/POSEIDON altimeter data. *Cont. Shelf Res.* **2004**, *24*, 1521–1529. [CrossRef]
49. Shi, W.; Wang, M.H. Satellite views of the bohai sea, yellow sea, and East China Sea. *Prog. Oceanogr.* **2012**, *104*, 10, 30–45. [CrossRef]
50. Fang, G.H. *Tides and Tidal Currents in East China Sea, Huanghai Sea and Bohai Sea. Oceanology of China Seas*; Springer: Houten, The Netherlands, 1994; pp. 101–112.
51. Zhang, M.; Tang, J.; Song, Q.; Dong, Q. Backscattering ratio variation and its implications for studying particle composition: A case study in Yellow and East China seas. *J. Geophys. Res.* **2010**. [CrossRef]
52. Andrews, S.W.; Nover, D.M.; Reuter, J.E.; Schladow, S.G. Limitations of laser diffraction for measuring fine particles in oligotrophic systems: pitfalls and potential solutions. *Water Resour. Res.* **2011**, *47*, 415–421. [CrossRef]
53. Lefebvre, J.P.; Ouillon, S.; Vinh, V.D.; Arfi, R.; Panché, J.Y.; Mari, X. Seasonal variability of cohesive sediment aggregation in the bach dang-cam estuary, haiphong (vietnam). *Geo-Mar. Lett.* **2012**, *2*, 103–121. [CrossRef]
54. Agrawal, Y.C.; Pottsmith, H.C. Instruments for particle size and settling velocity observations in sediment transport. *Mar. Geol.* **2011**, *168*, 89–114. [CrossRef]
55. Jouon, A.; Ouillon, S.; Douillet, P.; Lefebvre, J.P.; Fernandez, J.M.; Mari, X. Spatio-temporal variability in suspended particulate matter concentration and the role of aggregation on size distribution in a coral reef lagoon. *Mar. Geol.* **2008**, *256*, 36–48. [CrossRef]
56. Ahn, J.H.; Grant, S.B. Size distribution, sources, and seasonality of suspended particles in southern California marine bathing waters. *Environ. Sci. Technol.* **2007**, *41*, 695–702. [CrossRef] [PubMed]
57. Gartner, J.W.; Cheng, R.T.; Wang, P.-F.; Richter, K. Laboratory and field evaluations of the LISST-100 instrument for suspended particle size determinations. *Mar. Geol.* **2001**, *175*, 199–219. [CrossRef]
58. Karp-Boss, L.; Azevedo, L.; Boss, E. LISST-100 measurements of phytoplankton size distribution: Evaluation of the effects of cell shape. *Limnol. Oceanogr.* **2007**, *5*, 396–406. [CrossRef]
59. Serra, T.; Colomer, J.; Cristina, X.P.; Vila, X.; Arellano, J.B.; Casamitjana, X. Evaluation of laser in situ scattering instrument for measuring concentration of phytoplankton, purple sulfur bacteria, and suspended inorganic sediments in lakes. *J. Environ. Eng.* **2001**, *11*, 1023–1030. [CrossRef]

60. Agrawal, Y.; Traykovski, P. Particles in the bottom boundary layer: Concentration and size dynamics through events. *J. Geophys. Res.* **2001**. [CrossRef]
61. Sequoia Scientific, Inc. *LISST-100X Particle Size Analyzer, User's Manual Version 5.0*; Sequoia Scientific, Inc.: Bellevue, WA, USA, 2013.
62. Traykovski, P.; Latter, R.J.; Irish, J.D. A laboratory evaluation of the laser in situ scattering and transmissometery instrument using natural sediments. *Mar. Geol.* **1999**, *159*, 355–367. [CrossRef]
63. Agrawal, Y.; Whitmire, A.; Mikkelsen, O.A.; Pottsmith, H. Light scattering by random shaped particles and consequences on measuring suspended sediments by laser diffraction. *J. Geophys. Res. Oceans* **2008**. [CrossRef]
64. Milliman, J.D.; Meade, R.H. World-wide delivery of river sediment to the oceans. *J. Geol.* **1983**, *91*, 1–21. [CrossRef]
65. Wang, H.; Yang, Z.; Saito, Y.; Liu, J.P.; Sun, X. Interannual and seasonal variation of the Huanghe (Yellow River) water discharge over the past 50 years: Connections to impacts from ENSO events and dams. *Glob. Planet. Chang.* **2006**, *50*, 212–225. [CrossRef]
66. Xu, J. Variation of sediment flux to the sea in various grain size fractions in relation with the delta accretion of the Huanghe River in China. *Acta Oceanol. Sin.* **2006**, *28*, 88–97.
67. Zou, E.M.; Xiong, X.J.; Guo, B.H.; Lin, K. Characteristics and seasonal variations of the thermocline and halocline in the Huanghai Sea and the East China Sea. *J. Oceanogr. Huanghai Bohai Sea* **2001**, *19*, 8–18.
68. Fu, M.Z.; Wang, Z.L.; Sun, P.; Li, Y.; Li, R.X. Spatial distribution characteristics and the environmental regulation mechanisms of phytoplankton chlorophyll a in South Yellow Sea during summer 2006. *Acta Ecol. Sin.* **2009**, *29*, 5366–5375.
69. Zhou, H.; Zhang, Z.N.; Liu, X.S.; Tu, L.H.; Yu, Z.S. Changes in the shelf macrobenthic community over large temporal and spatial scales in the Bohai Sea, China. *J. Mar. Syst.* **2007**, *67*, 312–321. [CrossRef]
70. Mobley, C.D. *Light and Water-Radiative Transfer in Natural Waters*; Academic Press: San Diego, CA, USA, 1994.
71. Astoreca, R.; Doxaran, D.; Ruddick, K.; Rousseau, V.; Lancelot, C. Influence of suspended particle concentration, composition and size on the variability of inherent optical properties of the Southern North Sea. *Cont. Shelf Res.* **2012**, *35*, 117–128. [CrossRef]
72. Peng, T.; Qiu, Z.; Sun, D.; Wang, S. The study of suspended particulate matters particle size distribution based on the power-law model—A case study in the Yellow Sea and Bohai Sea. *Mar. Sci.* **2016**. [CrossRef]
73. Boredin, S.; Chang, C.W.; Liew, S.C. Effects of the suspended particle size distribution on water remote-sensing reflectance. In Proceedings of the 2013 IEEE International Geoscience and Remote Sensing Symposium, Melbourne, Australia, 21–26 July 2013.
74. Huang, J.; Chen, L.; Chen, X. Influence of suspended particle size distribution on the variability of water optical properties of the Poyang Lake, China. In Proceedings of the 2015 IEEE International Geoscience and Remote Sensing Symposium, Milan, Italy, 26–31 July 2015.
75. Nasiha, H.J.; Shanmugam, P.; Hariharasudhan, V.G. A new inversion model to estimate bulk refractive index of particles in coastal oceanic waters: Implications for remote sensing. *IEEE J. Sel. Top. Appl. Earth Obs. Remote Sens.* **2014**, *7*, 3069–3083. [CrossRef]
76. Nasiha, H.J.; Shanmugam, P. Estimating the bulk refractive index and related particulate properties of natural waters from remote-sensing data. *IEEE J. Sel. Top. Appl. Earth Obs. Remote Sens.* **2015**, *11*, 5324–5335. [CrossRef]